Journal of Materials Chemistry C

Accepted Manuscript

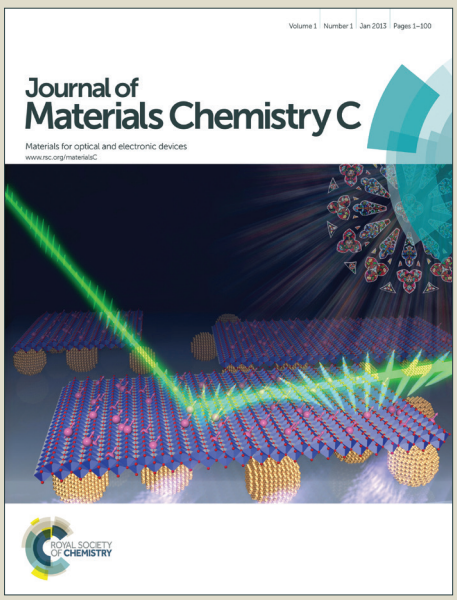

ROYAL SOCIETY OF CHEMISTRY

www.rsc.org/materialsC

Eu^{3+}@PMO: Synthesis, Characterization and Luminescence Properties.

Dolores Esquivel,[a] Anna M. Kaczmarek,[b] César Jiménez-Sanchidrián,[c] Rik Van Deun,[b] Francisco J. Romero-Salguero[c*] and Pascal Van Der Voort[a*]

[a] *Center for Ordered Materials, Organometallics & Catalysis, Krijgslaan 281-S3, 9000 Ghent, Belgium.*

[b] *L^3- Luminescent Lanthanide Lab, Department of Inorganic and Physical Chemistry, Ghent University, Krijgslaan 281-S3, 9000 Ghent, Belgium*

[c] *Department of Organic Chemistry, Nanochemistry and Fine Chemistry Research Institute (IUIQFN), Faculty of Sciences, University of Córdoba, Campus de Rabanales, Marie Curie Building, Ctra. Nnal. IV, km 396, 14071 Córdoba, Spain.*

* Corresponding authors: Tel.: +32 9 242 42 44. E-mail address: pascal.vandervoort@ugent.be (P. Van Der Voort). Tel.: +34 957212065. E-mail address: qo2rosaf@uco.es (F. J. Romero-Salguero).

Abstract

A periodic mesoporous organosilica (PMO) functionalized with dipyridyl-dihydropyridazine units has been successfully prepared by a hetero Diels-Alder reaction between the double bonds of an ethenylene-bridged PMO material and a substituted tetrazine. The ordering and mesoporosity of the parent material is maintained after the post-modification process, and the surface Diels-Alder adducts are clearly observable in the pores. These dipyridyl-dihydropyridazine moieties can form interesting chelates with lanthanide ions. Thus, two novel organic-inorganic luminescent hybrid materials have been obtained by linking of Eu^{3+} compounds to an ethene-PMO functionalized with dipyridyl-dihydropyridazine. Both materials have been studied in depth by photoluminescence spectroscopy and luminescence decay time measurements. Our results reveal the key role of surface Diels-Alder adducts as suitable sensitizing ligands for europium ions.

1. Introduction

Lanthanide materials have drawn a lot of attention because of their wide range of applications for example in bio-sciences, as catalysts, for lasers, and in lighting industry.[1-5] The interesting photophysical properties of lanthanide materials are largely due to the unique intra 4f transitions, which are only weakly influenced by the coordination environment or crystal field (caused by the shielding of the 4f orbitals by the filled 5s and 5p orbitals).[2, 6] Trivalent europium (Eu^{3+}) is often chosen as the doping ion to investigate the luminescence properties of a material because it shows strong emissions in the visible region. Eu^{3+} ions can also be used as a structural probe for investigating the local environment in a host material. However, one of the main problems with lanthanides considering their luminescence properties is the fact that lanthanide ions suffer from weak light absorption (the absorption coefficients are normally very low, $\varepsilon \approx 1–10\ M^{-1}\ cm^{-1}$). Therefore a very limited amount of radiation is absorbed when exciting directly into the 4f levels of the lanthanides. To overcome this, chromophores are often employed to transfer the absorbed energy more efficiently to the lanthanide ions. This is referred to as the "antenna effect". Some sensitizing ligands such as β-diketonates, aromatic carboxylates or heterocyclic ligands are considered good antenna molecules due to their excellent coordination ability and appropriate ligand-to-metal intracomplex energy transfer.[7-9] Unfortunately, the practical application has been limited due to their relatively poor stabilities under high pressure, high temperature or moisture conditions and their low mechanical strength.[10, 11] Thus, in recent years, numerous studies have been focusing on improving the photostability of lanthanide complexes through encapsulating them into a host structure, such as polymers[12-14], silica-based materials[15-18] and liquid crystals[19-21], to create organic-inorganic luminescent hybrid materials.[22]

Organic functionalized mesoporous silica materials have attracted particular attention as hybrid hosts for lanthanide complexes.[23-27] The post-synthetic ("grafting") or in-situ ("co-condensation") processes to introduce these functionalities have well-known limitations such as pore blocking, low organic loading or non-homogeneous distribution of the organic groups into the silica network. An alternative method to create organically functionalized mesoporous silicas, and thus overcoming successfully these drawbacks is the synthesis of periodic mesoporous organosilicas (PMOs).[28-30] These materials are synthesized using bridged organosilica precursors of the type $(R´O)_3$-Si-R-Si-$(OR´)_3$, with R´O a hydrolyzable group (e.g. methoxy or ethoxy groups) and R the organic bridging group, in the presence of a structure directing agent. Until now, numerous organic moieties, from simple compounds – methane, ethane, ethene or benzene – to more complex ones bearing different functionalities – thiol, tetrasulfide, metal complexes, chiral groups, ionic entities – have been successfully embedded into the silica framework.[31]

PMOs have a well-ordered mesoporous structure, a high hydrothermal and mechanical stability and a uniform distribution of the organic functionality into the pore walls. The presence of organic moieties in the framework of PMOs allows these materials to be modified and functionalized by using a whole array of organic reactions, giving rise to novel opportunities for designing advanced mesoporous materials. Phenylene-bridged PMOs have been mainly functionalized by electrophilic aromatic substitutions (sulfonation or nitration reactions) to incorporate acid or basic catalytic sites.[32-34] The -C=C- bonds on ethenylene-bridged PMOs have been functionalized to incorporate certain functionalities. Thiol and amine groups were incorporated on ethenylene-bridged PMOs by bromination of the unsaturated groups and subsequent nucleophilic substitution via either a Grignard reactant or via an amine containing a nucleophile, respectively. This

type of functionalized materials showed to be promising candidates for mercury or CO_2 adsorption.[35, 36] Epoxidation reactions on the ethenylene sites led to bifunctional (-SO_3H/-NH_2) catalysts through specific ring-opening reactions of the oxirane units.[37] Diels-Alder cycloadditions with common dienes (e.g. benzocyclobutene, anthracene and cyclopentadiene) followed by sulfonation of the resulting surface adducts were performed to generate new sulfonic acid functionalized PMO materials.[38, 39] Very recently, a vulcanization reaction was used for the first time on PMOs to introduce sulfur-containing functional groups.[40]

One of the main research interests of our group is to carry out different approaches to functionalize PMO materials. Thus, we have recently reported the incorporation of new surface N-heterocyclic compounds on periodic mesoporous organosilicas through Diels-Alder reactions with pyrrole derivatives.[41] The incorporation of N- containing moieties on the surface is highly interesting, not only because it yields advanced materials in catalysis and adsorption, but also because it is an attachment point to bind luminescent lanthanide complexes.[8] Up to date, only few studies have focused on the synthesis and luminescence properties of PMOs with chelating organic ligands for lanthanide ions. For instance, acridone and bipyridine moieties were successfully incorporated as bridging components within the silica framework in order to be used as light-harvesting antenna molecules for visible and near-infrared (NIR) emission, respectively.[42, 43] Moreover, novel organic-inorganic luminescent hybrid materials were obtained by linking lanthanide complexes to periodic mesoporous organosilicas functionalized with suitable sensitizing ligands, including mercaptobenzoic acid,[44] 1,10-phenanthroline,[45, 46] 2,2'-bipyridine[47] and 2-thenoyltrifluoroacetonate.[48]

Herein, we report the formation of surface nitrogen-based chelating heterocycles through hetero Diels-Alder reaction between the double bonds on an ethenylene-bridged PMO

and a tetrazine derivative. The presence of dipyridyl-dihydropyridazine components grafted onto the PMO surface as well as the preservation of the original ordering and mesoporosity is characterized in detail. An organic-inorganic luminescent hybrid material is obtained by complexation reaction of Eu^{3+} compounds, from either a solution of $EuCl_3 \cdot 6H_2O$ or a solution of $[Eu(tta)_3(H_2O)_2]$ complex (tta = 2-thenoyltrifluoroacetonate), with the resulting dipyridyl-dihydropyridazine functionalized ethene-PMO material. The luminescence properties of all the synthesized materials in the solid state are discussed.

2. Experimental Section

2.1. Chemicals. Grubb´s 1st generation catalyst, vinyltriethoxysilane, triblock copolymer $EO_{20}PO_{70}EO_{20}$ (Pluronic P123), 1-butanol (>99.7%), hydrochloric acid (37%) and acetone (>99.5%) were purchased from Sigma-Aldrich for the synthesis of the ethenylene-bridged PMO. A tetrazine derivative - 3,6-di-2-pyridyl-1,2,4,5-tetrazine - was obtained from Sigma-Aldrich to be used as diene for the Diels-Alder reaction. Dodecane (anhydrous, >99%, Sigma-Aldrich) and chloroform (Rotipuran, >99.5%, Carl Roth) were used as solvents in the chemical modification process. Europium(III) chloride ($EuCl_3 \cdot 6H_2O$, 99.9%) and methanol were obtained from Sigma-Aldrich for the grafting of lanthanide compounds onto the surface of the Diels-Alder adducts. All reactants and solvents were used as received without further purification.

2.2. Synthetic Procedures. *Synthesis of dipyridyl-dihydropyridazine functionalized ethenylene-bridged PMO (denoted as Dpdp-ePMO).* The parent 100% trans ethenylene-bridged PMO (ePMO) was synthesized according to the procedure reported by Van Der Voort et al.[49] The surface Diels-Alder reaction of e-PMO with the tetrazine derivative as

diene was carried out following a method already reported by our research group in the formation of surface Diels-Alder adducts on periodic mesoporous organosilicas.[39] Typically, 0.3 g of 100% trans ethenylene-bridged PMO (ePMO), previously heated under vacuum at 120ºC overnight, was added to a mixture of 0.25 g tetrazine derivative and 20 ml of dodecane. The resulting mixture was aged in an autoclave at 200ºC for 11 days. After cooling down, the solid was filtered and repeatedly washed with chloroform. In order to remove possible diene physically adsorbed into the pores, the material was refluxed in chloroform for 8h. After repeating this process twice, it was recovered by filtration, washed with chloroform and acetone and dried at 120ºC under vacuum. The nitrogen content on Dpdp-ePMO material was 2.39%.

Synthesis of Dpdp-ePMO material grafted with $EuCl_3$ (denoted as Dpdp-ePMO-$EuCl_3$). To prepare the Dpdp-ePMO-$EuCl_3$ material, a certain amount of $EuCl_3 \cdot 6H_2O$ was dissolved in methanol and then Dpdp-ePMO was added to this solution. The molar ratio of $EuCl_3 \cdot 6H_2O$: Dpdp-ePMO was 4 : 1. The total volume was approximately 20 mL. The mixture was stirred and heated on a heating block at 120°C for 24h. After the product had cooled down it was filtered and washed three times with methanol to guarantee the removal of physisorbed $EuCl_3 \cdot 6H_2O$ salt. Afterwards it was dried at 120ºC under vacuum.

Synthesis of Dpdp-ePMO material grafted with $Eu(tta)_3$ complex (denoted as Dpdp-ePMO-$Eu(tta)_3$). For the preparation of the Dpdp-ePMO-$Eu(tta)_3$ material first the $Eu(tta)_3$ complex was prepared according to a literature procedure.[50, 51] The obtained complex was characterized as a dihydrate $[Eu(tta)_3(H_2O)_2]$ by elemental analysis (calculated: 33.87% C, 15.03% O, 1.89% H; found: 33.94% C, 14.88% O, 2.10% H). A certain amount of the previously prepared $[Eu(tta)_3(H_2O)_2]$ complex was dissolved in methanol and then Dpdp-ePMO was added to this solution. Also in this case the molar ratio of $[Eu(tta)_3(H_2O)_2]$: Dpdp-ePMO was 4 : 1. The total volume was approximately

20 mL. The mixture was stirred and heated for 24h on a heating block at 120°C. After the product had cooled down it was filtered and washed three times with methanol to guarantee the complete removal of physisorbed Eu-tta complex. Afterwards it was dried at 120ºC under vacuum.

2.3. Characterization. Powder X-Ray diffraction (PXRD) patterns were recorded with an ARL X`TRA Diffractometer (Thermo Scientific) using Cu Kα radiation (40 kV and 30 mA). Nitrogen adsorption-desorption isotherms were measured by using a Micromeritics TriStar 3000 analyzer at -196ºC. The samples were vacuum dried for 24h at 120ºC before the measurements. Surface areas were calculated using the Brunauer-Emmett-Tellet (BET) method. Pore size distributions were obtained by analysis of the desorption branch of the isotherms using the Barrett-Joyner-Halenda (BJH) method. Diffuse reflectance infrared Fourier Transform (DRIFT) spectroscopy was performed on a Perkin-Elmer 2000 FTIR spectrometer. The sample was heated in situ from room temperature to 120ºC under vacuum in a diffuse reflectance environmental chamber (Harrick) connected to a temperature controller. The ^{13}C MAS NMR spectra were recorded at 100.61 MHz on a Bruker AVANCE-400 WB dual channel NMR spectrometer at room temperature. An overall of 1000 free induction decays were accumulated. The excitation pulse and recycle time were 6 μs and 2s. Chemical shifts were measured relative to tetramethylsilane standard. All samples were dried at 150ºC for 24h prior to analysis. Elemental analysis (CHNS) was performed on a Thermo Flash 2000 elemental analyzer by using V_2O_5 as catalyst.

Luminescence measurements. Photoluminescence measurements were done on an Edinburgh Instruments FLSP920 UV-vis-NIR spectrofluorimeter, using a 450W xenon lamp as the steady state excitation source and a Hamamatsu R928P PMT detector, which has a response curve between 200 and 900 nm. Luminescence decay times were recorded

using a 60W pulsed Xe lamp, operating at a frequency of 100 Hz. All steady-state measurements were carried out at a step size of 0.1 nm. The steady-state luminescence measurements presented in this manuscript were performed at room temperature. In order to compare the measurements the same amounts of powders were used as well as the same settings for each measurement (same step, slit size and dwell time). The CIE color coordinates, as well as color temperatures, were calculated using the ColorCalculater 4.97 freeware program provided by Osram Sylvania.

All presented emission spectra have been corrected for detector sensitivity. The excitation spectra have not been corrected for Xe-lamp spectrum. If the spectrum is corrected the short wavelength part of the spectrum (below 260 nm) is blown out of proportion, because the Xe-lamp has hardly any intensity at these wavelengths and as a result, the correction overcompensates.

3. Results and Discussion

The formation of surface dipyridyl-dihydropyridazine units on an ethenylene-bridged PMO material (ePMO) was achieved by Diels-Alder cycloaddition between the double bonds of the PMO (dienophile) and a substituted tetrazine (diene).[52, 53] The resulting material (Dpdp-ePMO) was used as a hybrid host material for lanthanide complexes, more specifically, of two europium compounds - $EuCl_3$ and $[Eu(tta)_3(H_2O)_2]$ -, giving rise to novel luminescent lanthanide hybrid materials (Dpdp-ePMO-$EuCl_3$ and Dpdp-ePMO-$Eu(tta)_3$) (Scheme 1).

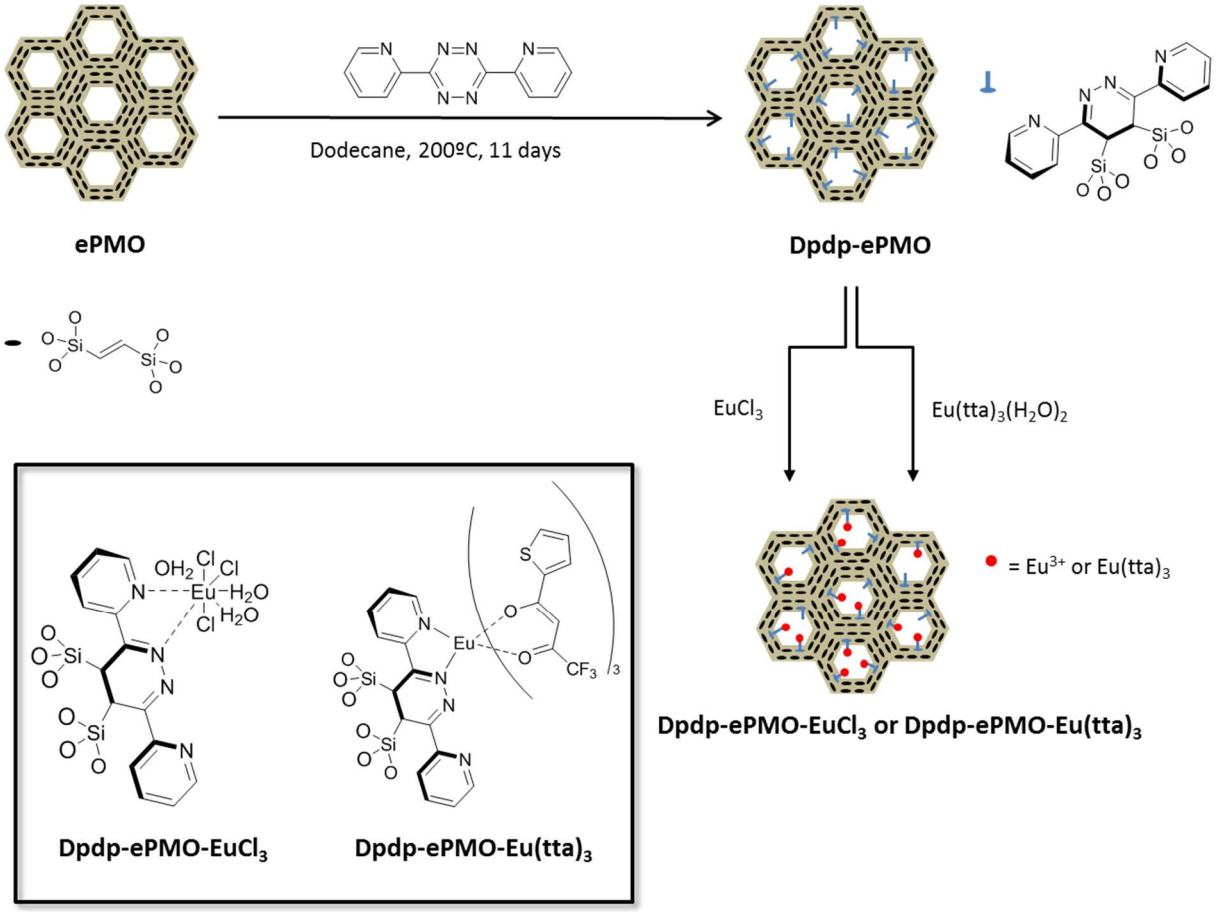

Scheme 1. Synthetic procedure for the formation of the surface Diels-Alder adducts (Dpdp-ePMO), and predicted structure of the resulting organic-inorganic luminescent hybrid mesoporous materials Dpdp-ePMO-$EuCl_3$ and Dpdp-ePMO-$Eu(tta)_3$.

3.1. Dipyridyl-dihydropyridazine functionalized parent material (Dpdp-ePMO).

The powder X-ray diffraction analysis performed on ePMO and Dpdp-ePMO are shown in Figure 1. After Diels-Alder reaction with the tetrazine derivative, Dpdp-ePMO exhibits a strong reflection (100) at low angle 2θ as well as two short second-order reflection peaks (110) and (200), typical of materials with a hexagonal arrangement of uniform pores. Compared with the X-ray diffraction pattern of the parent material (ePMO), that of Dpdp-ePMO is nearly unchanged, indicating that the ordered hexagonal mesostructure (P6mm) is retained after the hetero Diels-Alder reaction. However, a small shift in the first

reflection peak to a higher incidence angle is clearly observed in the sample Dpdp-ePMO. The resulting decrease in the d-spacing value, from 9.1 to 8.5 Å, suggests that there is a small shrinkage of the silicate network as consequence of the long thermal treatment used in the functionalization process (200ºC for 11 days).

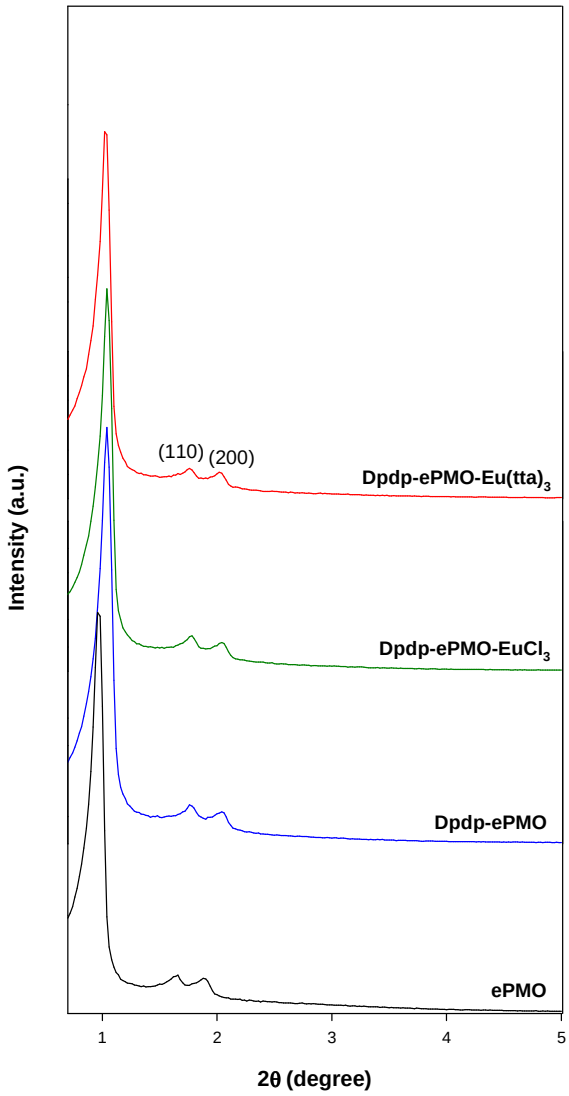

Figure 1. Powder X-ray diffraction patterns of ePMO, Dpdp-ePMO, Dpdp-ePMO-$EuCl_3$ and Dpdp-ePMO-$Eu(tta)_3$.

The N_2 adsorption/desorption isotherms of ePMO and Dpdp-ePMO are shown in Figure 2. Both samples exhibit type IV isotherms with H1-type hysteresis loops at relative pressures in the range of 0.4 – 0.8, characteristic of mesoporous materials with uniform

mesopores. The BET surface area (S_{BET}), pore volume (V), pore diameter (d) and wall thickness (t) are summarized in Table 1. It can be clearly seen that the surface area, pore volume and pore size are smaller after the formation of the Diels-Alder adduct. The S_{BET}, the pore volume and pore size decrease from 832 m^2 g^{-1}, 0.92 cm^3 g^{-1} and 6.3 Å for the parent material to 448 m^2 g^{-1}, 0.58 cm^3 g^{-1} and 5.1 Å for Dpdp-ePMO, respectively. However, a slight increase in the pore wall thickness (t) is observed due to the occupied volume by the surface organic groups. Thus, these results confirm the phenomenon of surface decoration inside the pores of the ePMO material with Diels-Alder adducts, previously observed in studies with other dienes.[38, 39]

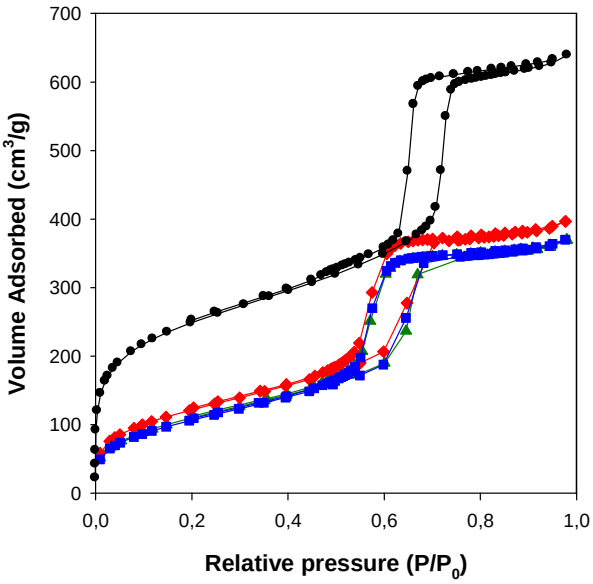

Figure 2. N_2 adsorption/desorption isotherms of ePMO (●), Dpdp-ePMO (■), Dpdp-ePMO-$EuCl_3$ (▲) and Dpdp-ePMO-$Eu(tta)_3$ (◆).

Table 1. Structural parameters[a]

Sample	d_{100} (nm)	S_{BET} (m^2g^{-1})	V (cm^3g^{-1})	d^b (nm)	t^c (nm)
ePMO	9.1	832	0.92	6.3	4.2
Dpdp-ePMO	8.5	448	0.58	4.8	5.0
Dpdp-ePMO-$EuCl_3$	8.5	406	0.56	4.8	5.0
Dpdp-ePMO-$Eu(tta)_3$	8.5	451	0.60	4.9	4.9

[a] d_{100}, (100) spacing; S_{BET}, BET surface area; V, pore volume; d, pore diameter; t, wall thickness.
[b] pore size by analysis of the desorption branch.
[c] calculated from ($a_0 - D_p$), where $a_0 = 2d_{100}/\sqrt{3}$

The presence of the surface Diels-Alder adduct has been confirmed by DRIFT and solid-state ^{13}C CP/MAS NMR measurements. Figure 3 depicts the DRIFT spectra of ePMO and Dpdp-ePMO. In the parent material, the bands at 2979 and 1577 cm^{-1} are assigned to =C-H and C=C stretching vibrations, respectively, characteristic of the ethenylene bridges inside the silica framework. After the Diels-Alder reaction with the tetrazine derivative, the resulting material exhibits some additional vibration bands corresponding to the new surface adducts. For instance, the bands at 3067 and 1667 cm^{-1} can be attributed to =C-H and C=N stretching, respectively. In addition, compared to the ePMO material, the Dpdp-ePMO material exhibits intense signals in the region 1360-1610 cm^{-1} which are characteristic of skeletal vibrations of N-heterocyclic components.

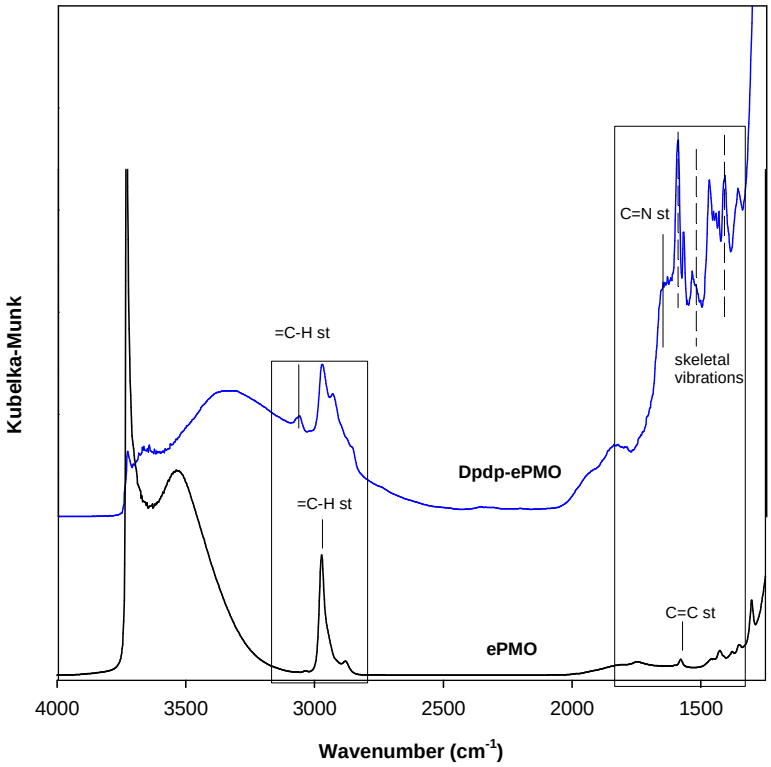

Figure 3. DRIFT spectra of ePMO and Dpdp-ePMO.

The solid-state ^{13}C CP/MAS NMR spectrum of the ePMO material displayed an intense signal at ca. 147 ppm, corresponding to the ethenylene units embedded inside the silica framework. Additional small signals at 17, 71 and 76 ppm are assigned to the residual surfactant Pluronic P123 remaining into the mesopores (Figure 4). The successful formation of the surface Diels-Alder adduct is proven by the presence of new signals in the aromatic region. These signals are due to unsaturated carbon atoms present in the surface adduct. In addition, the new upfield signal (δ = 30 ppm) has been assigned to the sp^3 carbons generated during the cycloaddition. Figure 4 depicts the assignments of these signals to the carbons of Dpdp-ePMO. Moreover, a small signal at ca. 57 ppm confirms the presence of the reaction intermediate with two N=N bonds (see Scheme S1, ESI†). The tetrazine derivative reacts with the double bonds of the ePMO in a sequence of a Diels-Alder reaction followed by retro Diels-Alder reaction. The signal at ca. 57 ppm

disappears from the spectrum of Dpdp-ePMO after treatment with $NaNO_2$,[54] giving further evidences of the successful modification through the Diels-Alder reaction (Figure S1, ESI†).

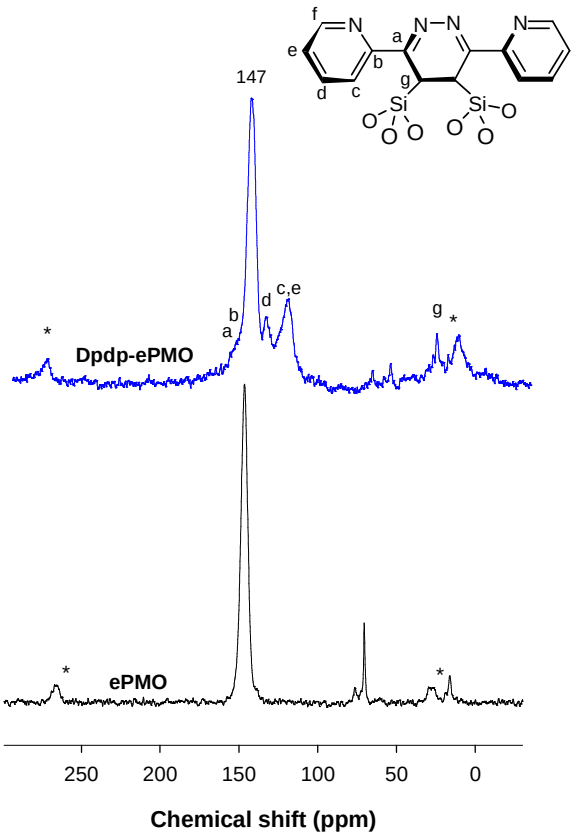

Figure 4. Solid-state ^{13}C CP/MAS NMR spectra of ePMO and Dpdp-ePMO.(* spinning sidebands).

3.2. $EuCl_3$ and $[Eu(tta)_3(H_2O)_2]$ bonded to dipyridyl-dihydropyridazine functionalized PMO. Structural characterization.

The Dpdp-ePMO material was selected as host material for the preparation of periodic mesoporous organosilicas bonded to $EuCl_3$ (Dpdp-ePMO-$EuCl_3$) and $[Eu(tta)_3(H_2O)_2]$ (Dpdp-ePMO-$Eu(tta)_3$). The powder X-ray diffraction patterns are presented in Figure 1. They show three well-resolved diffraction peaks in the 2θ range of 0.5 – 2, which can be

indexed as the (100), (110) and (200) reflections of a 2D-hexagonal structure. Compared to the X-ray diffraction pattern of Dpdp-ePMO, the d_{100}-spacing values of Dpdp-ePMO-$EuCl_3$ and Dpdp-ePMO-$Eu(tta)_3$ were nearly unchanged, indicating that the ordered hexagonal mesostructure remained intact after introducing the Eu^{3+} compound.

The N_2 adsorption-desorption isotherms of Dpdp-ePMO-$EuCl_3$ and Dpdp-ePMO-$Eu(tta)_3$ are depicted in Figure 2. Both samples display type-IV isotherms, characteristic of mesoporous materials with highly uniform size distributions. The structure data of these materials (BET surface area, total volume pore and pore size, etc.) are summarized in Table 1. After linking to the europium compounds, both materials maintained the surface properties of the parent material Dpdp-ePMO.

3.3. Photoluminescence properties of Eu-functionalized Dpdp-ePMO materials.

The excitation and emission spectra of Dpdp-ePMO-$EuCl_3$ are presented in Figure 5. The excitation spectrum consists of a strong broad band with a maximum at 302.0 nm, which can be attributed to the functionalized organic ligand. A weak band at around 393.0 nm can also be detected in the spectrum. It can be assigned to the $^5L_6 \leftarrow {}^7F_0$ transition of Eu^{3+}. When exciting the material at 302.0 nm the characteristic emission peaks of Eu^{3+} are visible in the emission spectrum, as well as a broad band, which partially overlaps these peaks. This band is due to the functionalized organic ligand; its presence in the emission spectrum indicates that the energy is not completely transferred from the organic ligand to the Eu^{3+} ions. The peaks labeled 1-5 have been assigned to electronic transitions in Table 2. It can be assumed that the observed emission arises by sensitizing the Eu^{3+} ions through the π-π^* transitions of the antenna ligand, because only very weak absorption bands of europium ($^5F_2 \leftarrow {}^7F_0$, $^5F_1 \leftarrow {}^7F_1$) occur at the corresponding excitation wavelength.

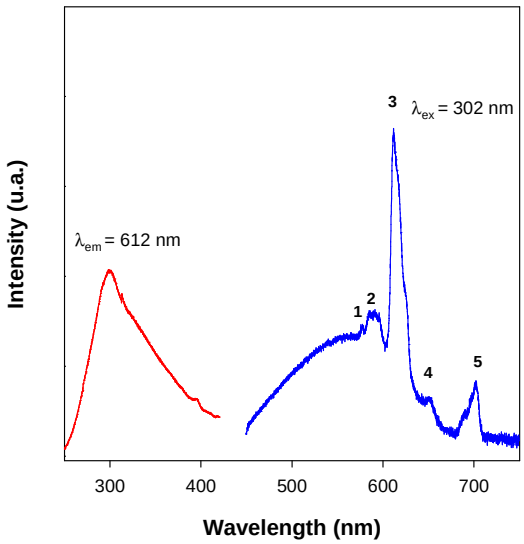

Figure 5. Excitation (red line) and emission (blue line) spectra of the Dpdp-ePMO-$EuCl_3$ material. The electronic transitions labeled 1-5 have been assigned in Table 2.

Table 2. Assignment of labeled transitions shown in Figure 5 and Figure 8.

Label	Dpdp-ePMO-$EuCl_3$	Wavelength (nm)	Energy (cm^{-1})	Dpdp-ePMO-$Eu(tta)_3$	Wavelength (nm)	Energy (cm^{-1})	Transition
1		578.0	17301		577.0	17331	$^5D_0 \rightarrow {}^7F_0$
2		591.0	16920		586.0	17065	$^5D_0 \rightarrow {}^7F_1$
3		612.0	16340		612.0	16340	$^5D_0 \rightarrow {}^7F_2$
4		652.0	15337		652.0	15337	$^5D_0 \rightarrow {}^7F_3$
5		702.0	14245		702.0	14245	$^5D_0 \rightarrow {}^7F_4$

To further investigate this, the Dpdp-ePMO-$EuCl_3$ material was excited at wavelengths ranging from 250 – 380 nm. No absorption of Eu^{3+} ions occurred at some of the chosen excitation wavelengths, yet Eu^{3+} emission peaks were observed. This verifies the presence of the antenna effect in this material. Figure 6 depicts the emission maps of the Dpdp-ePMO-$EuCl_3$ material excited at different wavelengths. The differences in emission intensity when excitation occurs at different wavelengths are clearly visible. However, it should be noted here that the emission intensity at short excitation wavelengths is most

likely underestimated because of the weak emission of the Xe-lamp at such short wavelengths.

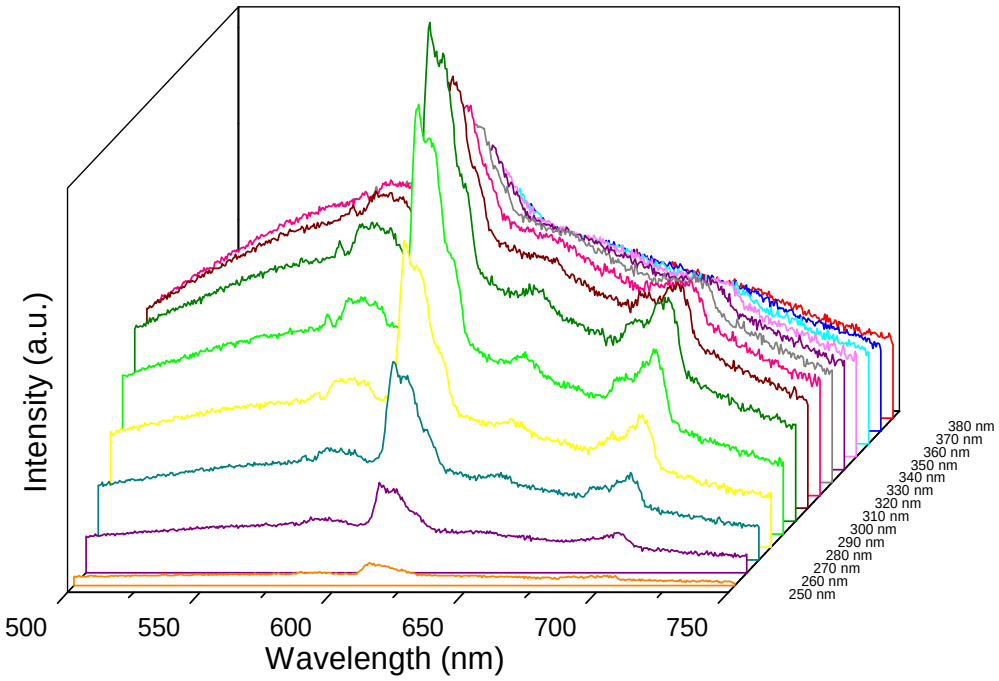

Figure 6. Emission maps of Dpdp-ePMO-$EuCl_3$ material excited at different wavelengths of the ligand band.

The CIE color coordinates of the sample excited at different wavelengths have been calculated based on the emission spectra data and color matching function issued by CIE in 1931. When exciting the sample at 302.0 nm it emits a yellow-orange color. The CIE coordinates have been calculated to be x = 0.4002, y = 0.4236. Usually a material doped with Eu^{3+} ions will emit red light, yet in this case there was also emission present from the organic ligand, which added a green-blue color component. Figure S2 shows the emission spectrum of Dpdp-ePMO-$EuCl_3$ plotted with a rainbow curve to show the different color components of the material, as well as the CIE coordinates projected on to a CIE chromaticity diagram. The change in CIE color coordinates upon excitation at different wavelengths has been presented in Table S1 (ESI†). As can be seen, there was

only a very slight change in the x and y coordinates as well as the color temperature (CCT - the color temperature, expressed in Kelvin degrees, indicates the tone of a specific light source).

The luminescence decay curve of Dpdp-ePMO-$EuCl_3$ was measured when excited at 302.0 nm and monitored at 612.0 nm. The decay curve of the Dpdp-ePMO-$EuCl_3$ material could be well fitted only when using a double-exponential function (Figure S3, ESI†). The lifetimes were calculated to be τ_1 = 105 (in 82%) µs and τ_2 = 466 µs (in 18%), indicating that the Eu^{3+} ions are located in two different environments in the obtained hybrid material.[43, 55] The lifetime of Eu^{3+} for Dpdp-ePMO-$EuCl_3$ was calculated as average lifetime (τ_{av})[56] yielding a value of 241 µs. From the resulting lifetime data shown in Table 3, we can discern that the average lifetimes of the pure $EuCl_3$bptz complex (Figure S4, ESI†) and the hybrid material are quite similar.

Table 3. Luminescent decay times of mesoporous materials.

	τ_1 (ms)/(%)	τ_2 (ms)/ (%)	τ_{av} (ms)	q (%)[b]
$EuCl_3$bptz[a]	0.239	-	0.239	-
Dpdp-ePMO-$EuCl_3$	0.105/82	0.466/18	0.241	1.9±0.2
$Eu(tta)_3$bptz[a]	0.476	-	0.476	-
Dpdp-ePMO-$Eu(tta)_3$	0.181/77	0.594/23	0.385	7.5±0.8

[a] $EuCl_3$bptz and $Eu(tta)_3$bptz were synthesize following the procedure from literature.[57] The decay curves for both pure complexes are well-fitted by a single exponential function.
[b]emission quantum yield

Moreover, a complex of Eu^{3+} with tta ligands has been prepared and grafted onto the Dpdp-ePMO material to investigate the luminescence. The tta ligand was chosen because it is known to be a very effective antenna ligand for Eu^{3+} ions.

The excitation and emission spectra of Dpdp-ePMO-Eu(tta)$_3$ are represented in Figure 7. The excitation spectrum consists of a strong broad band with a maximum at 298.0 nm which can be attributed to the organic ligands. Also a very weak Eu^{3+} peak is visible at around 396.0 nm and can be assigned to the $^5L_6 \leftarrow {}^7F_0$ transition. In the emission spectrum the characteristic $^5D_0 \rightarrow {}^7F_n$ (n = 0-4) transitions are present (see Table 2). Also a broad band, which partially overlapped with the Eu^{3+} peaks is present, but it is significantly weaker than in the case of Dpdp-ePMO-$EuCl_3$. This most likely suggests that in the Dpdp-ePMO-Eu(tta)$_3$ material, a more efficient energy transfer occurs from the organic ligands to the Eu^{3+} ions than in the Dpdp-ePMO-$EuCl_3$ material. In both materials (Dpdp-ePMO-$EuCl_3$ and Dpdp-ePMO-Eu(tta)$_3$), based on the observation that the $^5D_0$-$^7F_2$ transitions are dominant compared to the $^5D_0$-$^7F_1$ transitions, it can be stated that the europium ions are located in sites without inversion symmetry.

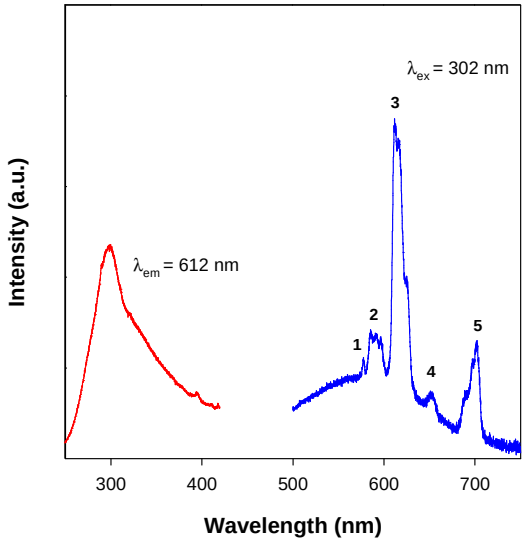

Figure 7. Excitation (red line) and emission (blue line) spectra of Dpdp-ePMO-Eu(tta)$_3$. The electronic transitions labeled 1-5 have been assigned in Table 2.

The Dpdp-ePMO-Eu(tta)$_3$ material was also excited at wavelengths ranging from 250 – 380 nm and the emission spectrum, as well as CIE coordinates and CCT (correlated color

temperature) were investigated. Figure 8 depicts the emission maps of the Dpdp-ePMO-Eu(tta)$_3$ material excited at different wavelengths. The differences in emission intensity when excitation occurs at different wavelengths can be clearly seen. Also here, the intensity at short wavelengths is most likely underestimated.

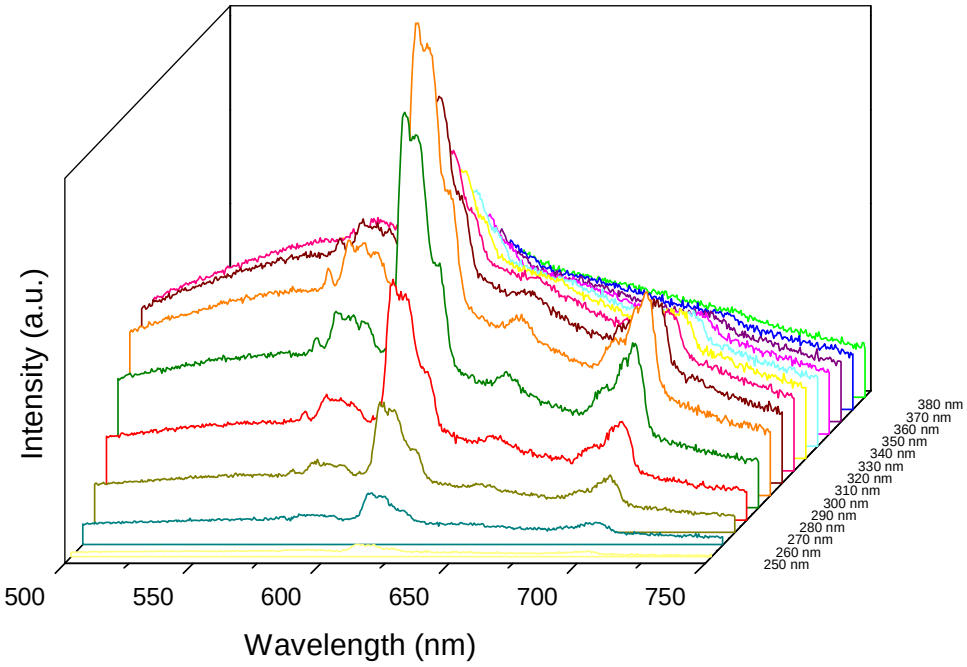

Figure 8. Emission maps of Dpdp-ePMO-Eu(tta)$_3$ material excited at different wavelengths of the ligand band.

When exciting the sample at 298.0 nm, it emits a red-orange color (compared to a yellow-orange color for the Dpdp-ePMO-EuCl$_3$ material) (see Figure S5). The CIE coordinates have been calculated to be x = 0.4945, y = 0.4871. The change in CIE color coordinates upon excitation at different wavelengths has been presented in Table S2 (ESI†). In this case, there is a more significant change in the x and y coordinates, as well as the CCT of the sample when exciting at different wavelengths. Some of the coordinates have also been shown on the CIE diagram in Figure 9 to show the change of emitted light when the sample was excited at different wavelengths.

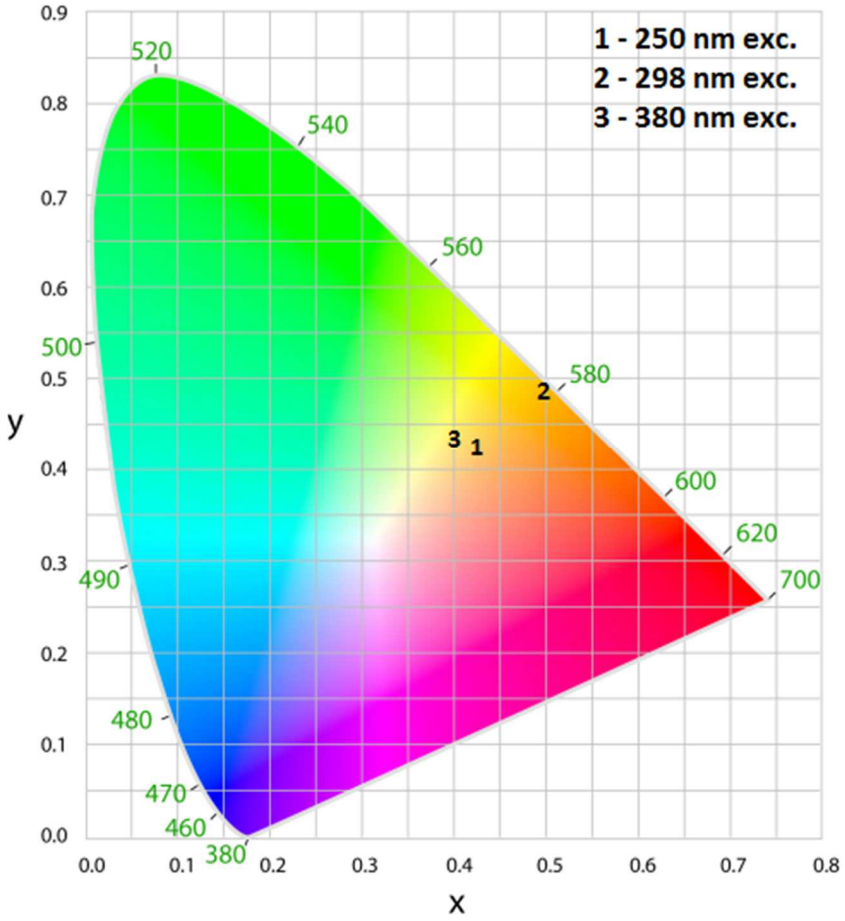

Figure 9. CIE color coordinates diagram presenting the approximate coordinates when Dpdp-ePMO-Eu(tta)$_3$ sample is excited at different wavelengths: 250 nm, 298 nm, and 380 nm. A change in color of the emitted light at different excitation wavelengths can be observed (CIE coordinates for other excitation wavelengths have been omitted for clarity).

The luminescence decay curve of Dpdp-ePMO-Eu(tta)$_3$ has been measured when exciting at 298.0 nm and monitoring at 612.0 nm. The decay curve of the Dpdp-ePMO-Eu(tta)$_3$ material could be well fitted only when using a double-exponential function (see Figure S6, ESI†). The lifetimes have been calculated to be τ_1 = 0.181 (in 77%) ms and τ_2 = 0.594 ms (in 23%). The presence of two lifetimes in this case also suggests that the Eu^{3+} ions are located in two different coordination environments. The corresponding average

lifetime τ_{av} in Dpdp-ePMO-Eu(tta)$_3$ material is 0.385 ms. For comparison, the decay curve of the pure Eu(tta)$_3$bptz complex exhibits a single exponential profile with a lifetime of 0.476 ms (Figure S7, ESI† and Table 3). The shorter lifetime of Dpdp-ePMO-Eu(tta)$_3$, compared with that of pure complex Eu(tta)$_3$bptz, can be due to a possible quenching by the O-H in the silanol groups of the PMO matrix in hybrid materials. However, Dpdp-ePMO-Eu(tta)$_3$ shows a longer lifetime than Dpdp-ePMO-EuCl$_3$ which indicates that the β-diketone (tta) is a more efficient sensitizer, which can replace part of the water molecules coordinated to the Eu^{3+} ions, improving the luminescent properties of the resulting hybrid material. In addition, Dpdp-ePMO-Eu(tta)$_3$ exhibited a quantum yield value of 7.5 ± 0.1, much higher than that obtained for Dpdp-ePMO-EuCl$_3$. The quantum yield value of the Dpdp-ePMO-Eu(tta)$_3$ sample is comparable with the value reported by Biju et al.[48] In that work a 4,4'-biphenylene-bridged mesoporous organosilica framework functionalized with 2-thenoyltrifluoroacetone to which lanthanide ions are bonded is reported. For the Eu-PMO material they reported a quantum yield of 7.7%, so perfectly comparable to the value found for our material. To the best of our knowledge this is one of the few papers where the absolute quantum yield of a Eu-PMO material is reported.

Conclusions

In summary, a new nitrogen-chelating heterocyclic compound has been successfully incorporated on the surface of an ethenylene-bridged periodic mesoporous organosilica through a hetero Diels-Alder reaction. Its complete characterization by powder X-ray diffraction, DRIFT, N_2 adsorption-desorption and ^{13}C NMR confirmed the formation of these surface Diels-Alder adducts as well as the preservation of the ordered mesostructure of the parent material. The resulting material was selected as a hybrid host material for

Eu^{3+} compounds. Thus, two novel organic-inorganic mesoporous luminescent hybrid materials were prepared by bonding the Eu-compounds ($EuCl_3 \cdot 6H_2O$ or $[Eu(tta)_3(H_2O)_2]$) to ethene-PMO functionalized with dipyridyl-dihydropyridazine moieties. Both resulting materials - Dpdp-ePMO-$EuCl_3$ and Eu Dpdp-ePMO-$Eu(tta)_3$ – showed the characteristics emission peaks of Eu^{3+} in the emission spectrum. Nevertheless, the more efficient energy transfer in the Dpdp-ePMO-$Eu(tta)_3$ suggests that the surface Diels-Alder adducts (dipyridyl-dihydropyridazine moieties) along with the sensitizing β-diketone (tta) ligands can act as feasible antenna ligands to sensitize the Eu^{3+} ions.

Acknowledgements

D. E. gratefully acknowledges the FWO-Vlaanderen (Fund Scientific Research – Flanders, grant number 3E10813W) as postdoctoral researcher for the financial support. F. J. R.-S. and C. J.-S. acknowledge funding of this research by the Spanish Ministry of Economy and Competitiveness (Project MAT2013-44463-R), Andalusian Regional Government (FQM-346 group), and Feder Funds. R. V. D. thanks the Hercules Foundation (project AUGE/09/024 “Advanced Luminescence Setup”) and Ghent University (UGent; project BOF 01N01010) for funding.

References

1. L. Armelao, S. Quici, F. Barigelletti, G. Accorsi, G. Bottaro, M. Cavazzini and E. Tondello, *Coord Chem Rev*, 2010, 254, 487-505.
2. K. Binnemans, *Chem Rev*, 2009, 109, 4283-4374.
3. G. Blasse and B. C. Grabmaier, *Luminescent Materials*, 1994, Springer Verlag, Berlin.
4. H. Y. He, H. Q. Ma, D. Sun, L. L. Zhang, R. M. Wang and D. F. Sun, *Cryst Growth Des*, 2013, 13, 3154-3161.
5. T. N. Parac-Vogt, K. Deleersnyder and K. Binnemans, *J Alloy Compd*, 2004, 374, 46-49.
6. J. C. G. Bunzli and C. Piguet, *Chem Soc Rev*, 2005, 34, 1048-1077.
7. V. Bekiari and P. Lianos, *Adv Mater*, 1998, 10, 1455-1458.
8. N. Sabbatini, M. Guardigli and J. M. Lehn, *Coord Chem Rev*, 1993, 123, 201-228.
9. N. Sabbatini, A. Mecati, M. Guardigli, V. Balzani, J. M. Lehn, R. Zeissel and R. Ungaro, *J Lumin*, 1991, 48-9, 463-468.
10. S. V. Eliseeva and J. C. G. Bunzli, *Chem Soc Rev*, 2010, 39, 189-227.
11. J. Feng and H. J. Zhang, *Chem Soc Rev*, 2013, 42, 387-410.

12. L. D. Carlos and A. L. L. Videira, *Phys Rev B*, 1994, 49, 11721-11728.
13. L. H. Wang, W. Wang, W. G. Zhang, E. T. Kang and W. Huang, *Chem Mater*, 2000, 12, 2212-2218.
14. C. Y. Yang, V. Srdanov, M. R. Robinson, G. C. Bazan and A. J. Heeger, *Adv Mater*, 2002, 14, 980-+.
15. P. P. Lima, R. A. S. Ferreira, R. O. Freire, F. A. A. Paz, L. S. Fu, S. Alves, L. D. Carlos and O. L. Malta, *Chemphyschem*, 2006, 7, 735-746.
16. H. R. Li, N. N. Lin, Y. G. Wang, Y. Feng, Q. Y. Gan, H. J. Zhang, Q. L. Dong and Y. H. Chen, *Eur J Inorg Chem*, 2009, 519-523.
17. H. R. Li, J. Lin, H. J. Zhang, L. S. Fu, Q. G. Meng and S. B. Wang, *Chem Mater*, 2002, 14, 3651-3655.
18. M. R. Felicio, T. G. Nunes, P. M. Vaz, A. M. P. Botas, P. Ribeiro-Claro, R. A. S. Ferreira, R. O. Freire, P. D. Vaz, L. D. Carlos, C. D. Nunes and M. M. Nolasco, *J Mater Chem C*, 2014, DOI: DOI: 10.1039/c4tc01072h.
19. K. Binnemans and C. Gorller-Walrand, *Chem Rev*, 2002, 102, 2303-2345.
20. R. Van Deun, D. Moors, B. De Fre and K. Binnemans, *J Mater Chem*, 2003, 13, 1520-1522.
21. K. Lunstroot, K. Driesen, P. Nockemann, C. Gorller-Walrand, K. Binnemans, S. Bellayer, J. Le Bideau and A. Vioux, *Chem Mater*, 2006, 18, 5711-5715.
22. B. Yan, *Rsc Adv*, 2012, 2, 9304-9324.
23. J. Graffion, X. Cattoen, M. W. C. Man, V. R. Fernandes, P. S. Andre, R. A. S. Ferreira and L. D. Carlos, *Chem Mater*, 2011, 23, 4773-4782.
24. Y. J. Gu and B. Yan, *Eur J Inorg Chem*, 2013, 2963-2970.
25. X. M. Guo, H. D. Guo, L. S. Fu, R. P. Deng, W. Chen, J. Feng, S. Dang and H. J. Zhang, *J Phys Chem C*, 2009, 113, 2603-2610.
26. Y. Li, B. Yan and H. Yang, *J Phys Chem C*, 2008, 112, 3959-3968.
27. D. Wang, B. Li, L. M. Zhang, J. Ying and X. D. Wu, *J Lumin*, 2010, 130, 598-602.
28. T. Asefa, M. J. MacLachlan, N. Coombs and G. A. Ozin, *Nature*, 1999, 402, 867-871.
29. S. Inagaki, S. Guan, Y. Fukushima, T. Ohsuna and O. Terasaki, *J Am Chem Soc*, 1999, 121, 9611-9614.
30. B. J. Melde, B. T. Holland, C. F. Blanford and A. Stein, *Chem Mater*, 1999, 11, 3302-3308.
31. P. Van Der Voort, D. Esquivel, E. De Canck, F. Goethals, I. Van Driessche and F. J. Romero-Salguero, *Chem Soc Rev*, 2013, 42, 3913-3955.
32. D. Esquivel, C. Jimenez-Sanchidrian and F. J. Romero-Salguero, *J Mater Chem*, 2011, 21, 724-733.
33. S. Inagaki, S. Guan, T. Ohsuna and O. Terasaki, *Nature*, 2002, 416, 304-307.
34. M. Ohashi, M. P. Kapoor and S. Inagaki, *Chem Commun*, 2008, 841-843.
35. E. De Canck, L. Lapeire, J. De Clercq, F. Verpoort and P. Van Der Voort, *Langmuir*, 2010, 26, 10076-10083.
36. E. De Canck, I. Ascoop, A. Sayari and P. Van Der Voort, *Phys Chem Chem Phys*, 2013, 15, 9792-9799.
37. M. Sasidharan, S. Fujita, M. Ohashi, Y. Goto, K. Nakashima and S. Inagaki, *Chem Commun*, 2011, 47, 10422-10424.
38. K. Nakajima, I. Tomita, M. Hara, S. Hayashi, K. Domen and J. N. Kondo, *Adv Mater*, 2005, 17, 1839-1842.
39. D. Esquivel, E. De Canck, C. Jimenez-Sanchidrian, P. Van Der Voort and F. J. Romero-Salguero, *J Mater Chem*, 2011, 21, 10990-10998.
40. M. I. Lopez, D. Esquivel, C. Jimenez-Sanchidrian, P. Van Der Voort and F. J. Romero-Salguero, *J. Phys. Chem. C*, 2014, 118, 17862−17869.
41. D. Esquivel, E. De Canck, C. Jiménez-Sanchidrián, F. J. Romero-Salguero and P. Van Der Voort, *MaterChemPhys*, 2014, 148, 403-410.

42. H. Takeda, Y. Goto, Y. Maegawa, T. Ohsuna, T. Tani, K. Matsumoto, T. Shimada and S. Inagaki, *Chem Commun*, 2009, 40, 6032-6034.
43. L. N. Sun, W. P. Mai, S. Dang, Y. N. Qiu, W. Deng, L. Y. Shi, W. Yan and H. J. Zhang, *J Mater Chem*, 2012, 22, 5121-5127.
44. Y. Li, B. Yan and Y. J. Li, *Micropor Mesopor Mat*, 2010, 132, 87-93.
45. X. M. Guo, X. M. Wang, H. J. Zhang, L. S. Fu, H. D. Guo, J. B. Yu, L. D. Carlos and K. Y. Yang, *Micropor Mesopor Mat*, 2008, 116, 28-35.
46. B. Yan and Y. J. Gu, *Inorg Chem Commun*, 2013, 34, 75-78.
47. H. Takeda, M. Ohashi, T. Tani, O. Ishitani and S. Inagaki, *Inorg Chem*, 2010, 49, 4554-4559.
48. S. Biju, Y. K. Eom, J. C. G. Bunzli and H. K. Kim, *J Mater Chem C*, 2013, 1, 3454-3466.
49. C. Vercaemst, M. Ide, B. Allaert, N. Ledoux, F. Verpoort and P. Van Der Voort, *Chem Commun*, 2007, 22, 2261-2263.
50. L. R. Melby, E. Abramson, J. C. Caris and N. J. Rose, *J Am Chem Soc*, 1964, 86, 5117-&.
51. K. Binnemans, P. Lenaerts, K. Driesen and C. Gorller-Walrand, *J Mater Chem*, 2004, 14, 191-195.
52. R. A. Carboni and R. V. Lindsey, *J Am Chem Soc*, 1959, 81, 4342-4346.
53. J. Sauer, *B Soc Chim Belg*, 1992, 101, 521-540.
54. G. P. Sagitullina, L. V. Glyzdinskaya and R. S. Sagitullin, *Khim Geterotsikl+*, 2005, 858-863.
55. J. B. Yu, R. P. Deng, L. N. Sun, Z. F. Li and H. J. Zhang, *J Lumin*, 2011, 131, 328-335.
56. S. Buddhudu, M. Morita, S. Murakami and D. Rau, *J Lumin*, 1999, 83-4, 199-203.
57. N. M. Shavaleev, S. J. A. Pope, Z. R. Bell, S. Faulkner and M. D. Ward, *Dalton T*, 2003, DOI: Doi 10.1039/B300294b, 808-814.

Graphical abstract

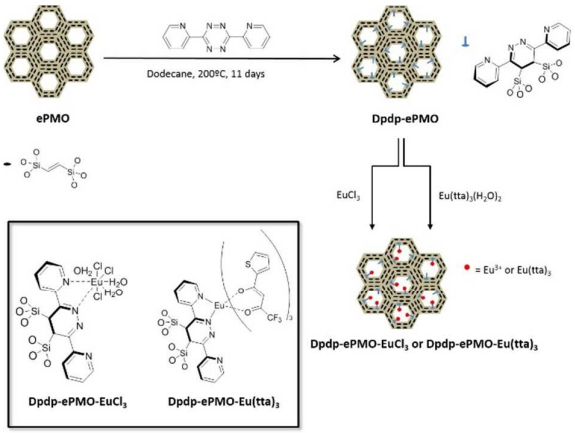

Two novel organic-inorganic luminescent hybrid materials have been obtained by linking of Eu^{3+} compounds to an ethene-PMO functionalized with dipyridyl-dihydropyridazine.